IEEE Access
Multidisciplinary | Rapid Review | Open Access Journal

Received 27 July 2022, accepted 15 August 2022, date of publication 29 August 2022, date of current version 9 September 2022.

Digital Object Identifier 10.1109/ACCESS.2022.3202886

APPLIED RESEARCH

Design of Wideband Continuous Class-F Power Amplifier Using Low Pass Matching Technique and Harmonic Tuning Network

MD. GOLAM SADEQUE[1,6], (Member, IEEE), ZUBAIDA YUSOFF[1], (Senior Member, IEEE), SHAIFUL JAHARI HASHIM[2], AZAH SYAFIAH MOHD MARZUKI[3], (Senior Member, IEEE), JONATHAN LEES[4], (Senior Member, IEEE), AND DOMINIC FITZPATRICK[5], (Senior Member, IEEE)

[1]Faculty of Engineering, Multimedia University, Cyberjaya, Selangor 63100, Malaysia
[2]Faculty of Engineering, Universiti Putra Malaysia, Serdang, UPM Selangor 43400, Malaysia
[3]TM R&D Sdn Bhd, Cyberjaya, Selangor 63000, Malaysia
[4]Centre of High Engineering, Cardiff University, Cardiff CF24 3AA, U.K.
[5]Ametek-CTS, Ryde PO33 2BE, U.K.
[6]Department of Electrical, Electronic and Communication Engineering, Pabna University of Science and Technology, Pabna 6600, Bangladesh

Corresponding author: Zubaida Yusoff (zubaida@mmu.edu.my)

This work was supported in part by the Fundamental Research Grant Scheme (FRGS) Fund through the Malaysian Ministry of Higher Education Malaysia (MOHE) under Grant FRGS/1/2019/TK04/MMU/02/15.

ABSTRACT Many countries have allocated new frequency bands for fifth generation (5G) communication systems. In this paper, a wideband continuous class-F (CCF) radio frequency power amplifier (RFPA) is presented for the new 5G frequency band, from 3.3 GHz to 4.3 GHz using a 10 W Cree CGH40100F device. A unique wideband RFPA design approach for the output matching network (OMN) is also presented by applying a harmonic tuning network (HTN) for the harmonics and a low pass matching technique (LPMT) for the fundamental frequency. The RFPA is fabricated, and promising measurement results show a drain efficiency of 55.9% to 65.3% is achieved at an output power of 40 dBm (± 0.3 dBm) over a frequency range of 3.3 GHz to 4.3 GHz. A two-tone signal with a 10 MHz spacing was also applied to investigate the linearity of the RFPA.

INDEX TERMS GaN HEMT, 5G communication, wideband, high efficiency, radio frequency power amplifier (RFPA), low pass matching, current generator plane (I-Gen).

I. INTRODUCTION

Wireless communication develops rapidly to meet the demands of users. The radio frequency power amplifier (RFPA) has become a critical component in wireless communication systems [1]. Fifth-generation (5G) wireless communication systems require wideband and high-efficiency RFPAs. One of the main challenges in the existing communication systems is the shortage of spectrum resources. For this reason, for the past few years, the problem of the spectrum distribution has drawn the attention of researchers and government departments such as the Federal Communications Commission (FCC). The 5G communication network will primarily operate in two frequency bands: a high-frequency band between 24 GHz and 86 GHz and a low-frequency band till 6 GHz [2]. In the low-frequency band below 6 GHz, different countries' communication networks will use various frequencies of operation. The government of some countries nominated the frequency bands for the operation of the 5G system. The frequency of these countries is listed in [3], showing the lowest operating frequency of 3.3 GHz and the highest operating frequency of 4.3 GHz. In order to implement a 5G communications system, a wideband RFPA is needed for the frequency band of 3.3-4.3 GHz.

RFPAs are categorized into two main types: linear mode and switching mode [4]. During recent decades, different types of narrowband RFPA modes have been explored theoretically and experimentally [5]. Different modes of RFPAs

The associate editor coordinating the review of this manuscript and approving it for publication was Adamu Murtala Zungeru.

are created by applying waveform engineering at the current generator (I-Gen) plane that is inside the device and is different from the package/measurement plane. The package plane is a reference plane where the voltage and current waveform is actually measured. The operating modes of transistors can be defined by identifying the drain voltage and current waveforms at the I-Gen plane. Therefore, the performance parameters of the RFPA such as efficiency, gain, and output power can be optimized by shaping the drain voltage and current waveforms at the I-Gen plane. Numerous types of high-efficiency RFPAs exist in reality based on the harmonic-tuned circuit, such as class-E, class-F/F^{-1}, and class-J [6]. From the classical class-B condition, the fundamental theory of class-F and inverse class-F RFPA is developed. Class-F RFPAs can achieve high efficiency for a narrowband, which is usually less than 10% [6]. So, to solve the issue of narrowband, continuous mode RFPAs i.e. continuous class-F (CCF), continuous inverse class-F (CCF^{-1}) and continuous class-J (CCJ) have been discovered and these modes can be accomplished by properly controlling the impedance termination of the fundamental as well as the harmonic frequencies [7]. The continuous mode harmonic tuned RFPA has been proved to be a good solution for extending the bandwidth while maintaining good efficiency [1]. However, there is a limitation to the CCF RFPA when dealing with the anticlockwise rotation of the second harmonic impedance, it is difficult to match such impedance trajectory using passive matching networks [8]. Consequently, the second harmonic's impedance is matched carefully because appropriate matching of the optimum impedance of the fundamental and harmonic frequencies is important for the continuous mode RFPA. Many impedance matching techniques have been explored and developed to date. One of the most effective methods is the low pass matching technique (LPMT).

Most recent studies of CCF RFPAs focused on frequencies lower than 3.6 GHz [8], [9], [10], [11], [12], [13], [14], whereas in this paper, the RFPA design extends the application of CCF mode for the 5G system whose frequency range from 3.3 GHz to 4.3 GHz that is the first in the literature to the best of the authors knowledge. This paper also presents a new design approach to achieve a wideband matching network for the CCF RFPA. The new design approach for this work has the following methodology. First, to manage the harmonic impedances, a harmonic tuning network (HTN) is designed. Then, using the LPMT, the optimum fundamental impedances over the band are synthesized. The same matching technique is applied to both the input and output of the Cree device. When tuning is performed to get better performance, importance is given to the efficiency and the output power while keeping the signal distortion low enough to meet the spectral mask required by the regulatory authority. The linearity of the RFPA can be quantified by various metrics such as third order intermodulation distortion (IMD3) product, third-order intercept point (TOI), and 1-dB compression point [15]. To determine the linearity of the designed RFPA, a 10 MHz spacing two-tone signal is applied at the input to test the fabricated RFPA, and IMD3 is measured over the band of frequency from 3.3 GHz to 4.3 GHz.

The organization of this paper is as follows. Section II shows the theoretical derivation of the fundamental as well as harmonic impedances for the CCF RFPA. The impedance of this mode is derived from the equation of the drain voltage and current waveforms of the classical class-B mode RFPA. Section III elaborates the design methodology of the output matching network (OMN) and the input matching network (IMN). The design methodology is implemented considering the optimum impedance at the device package plane. To achieve the design goals, the HTN and fundamental frequency impedance matching networks are designed separately. In Section V, the measurement of the fabricated RFPA is presented for the frequency band of 3.3 GHz to 4.3 GHz. Section VI has the conclusions.

II. FUNDAMENTAL AND HARMONIC IMPEDANCES OF CCF MODE THEORETICAL DERIVATION

By appropriately terminating impedance at the I-Gen plane of the active device at the fundamental and harmonic frequencies, the conventional class-F RFPA is produced from the classical class-B RFPA [16]. The drain current waveform of a class-B RFPA is a half-rectified sinusoidal wave [17]. The drain current i_D of the class-B RFPA for an infinite number of frequencies is described by the following equation:

$$\begin{aligned} i_D &= I_{\max}\cos\theta, \ -\frac{\pi}{2} < \theta < \frac{\pi}{2} \\ &= 0, \ -\pi < \theta \le -\frac{\pi}{2}; \quad \frac{\pi}{2} \le \theta \le \pi \end{aligned} \tag{1}$$

where I_{max} is the drain current's maximum value and θ is the angle of conduction of the device.

The conventional class-F RFPA is obtained ideally by having open-circuited termination at odd harmonics and short-circuited termination at even harmonics, as shown in Figure 1(a). This ensures that the voltage waveform will be a perfect square wave and the current waveform will be a half-rectified sinusoidal waveform, as shown in Figure 1(b). The theoretical efficiency of class-F RFPA is 100 percent since the drain voltage and current waveforms do not overlap. Usually, the device is terminated up to the third harmonic only, corresponding to the current and voltage waveforms, because if the harmonic tuning is increased beyond the third harmonic, it increases the circuit complexity and insertion loss of the load network [18] without any significant improvement in the efficiency. In the case of the conventional class-F RFPAs, the coefficient of the normalized waveform of the drain voltage up to the third harmonic can be calculated in two ways: by considering the flat waveform [19] and by considering the maximum efficiency [20]. In this paper, the coefficient of voltage waveform is calculated by considering maximum efficiency. In this case, when the termination of harmonics is restricted to three, the theoretical efficiency drops from 100% to 90.70% [21]. The Fourier series of the drain voltage, v_D, normalized by V_{DC} up to the third harmonic as given in [14]

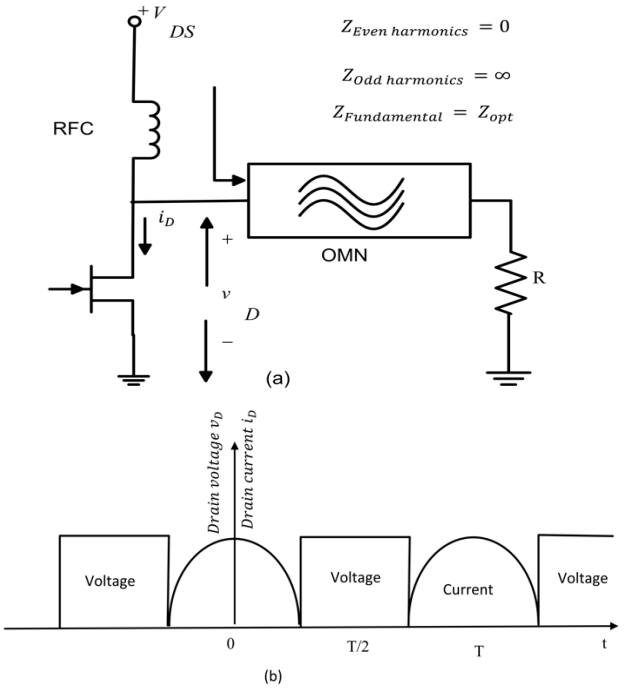

FIGURE 1. (a) Class-F RFPA output circuit and (b) the corresponding ideal waveform.

is as follows:

$$v_D = 1 - \frac{2}{\sqrt{3}}\cos\theta + \frac{1}{3\sqrt{3}}\cos 3\theta \tag{2}$$

To address the problem of narrowband performance of class-F and inverse class-F amplifiers, Cripps [22] introduced a continuous mode of operation. To get a CCF RFPA, a factor of $(1 - \gamma \sin\theta)$ is used to multiply the equation of the drain voltage. The equation can be extended as follows:

$$v_D = \left(1 - \frac{2}{\sqrt{3}}\cos\theta + \frac{1}{3\sqrt{3}}\cos 3\theta\right)(1 - \gamma \sin\theta) \tag{3}$$

where γ denotes the design space factor. The factor γ is swept from -1 to +1 to maintain a positive drain voltage. For $\gamma = 0$, the standard conventional class-F RFPA is obtained. This CCF mode provides a series of optimal impedances for different values of γ, and for any values of γ within the range, the efficiency of the CCF is the same as the conventional class-F RFPA. For $\gamma = -1$ to $+1$, a family of the drain voltage is obtained and the corresponding half-rectified sinusoidal current waveforms are shown in Figure 2. The harmonic impedances of the CCF RFPA are shown in the following equations derived from the drain current (1) and the drain voltage (3),

$$Z_F = R_{opt}\frac{2}{\sqrt{3}} + j\gamma R_{opt}$$
$$Z_{2F} = -jR_{opt}\frac{7\sqrt{3}\pi}{24}\gamma$$
$$Z_{3F} = \infty$$

$$R_{opt} = \frac{V_{DC} - V_{knee}}{I_{\max/2}} \tag{4}$$

where R_{opt} is the matching impedance at the optimum condition for the classical class-B operation. For an ideal case, $V_{knee} = 0$ while V_{DC} and I_{max} represent the biasing voltage of the drain and the maximum drain current of the transistor, respectively. As the space factor, γ, goes from –1 to +1, the fundamental impedance varies on the constant resistance circle in a clockwise direction, and the impedance of the second harmonic is located on the Smith chart's edge and rotates anticlockwise, but the impedance of third harmonics remains fixed at infinite resistance point of the Smith chart (see Figure 3).

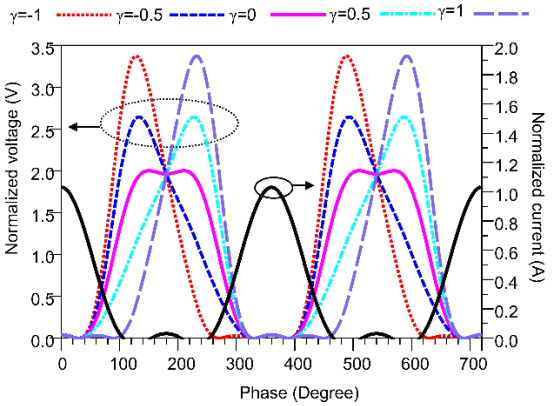

FIGURE 2. Normalized current and voltage waveform of the CCF RFPA for $-1 < \gamma < 1$.

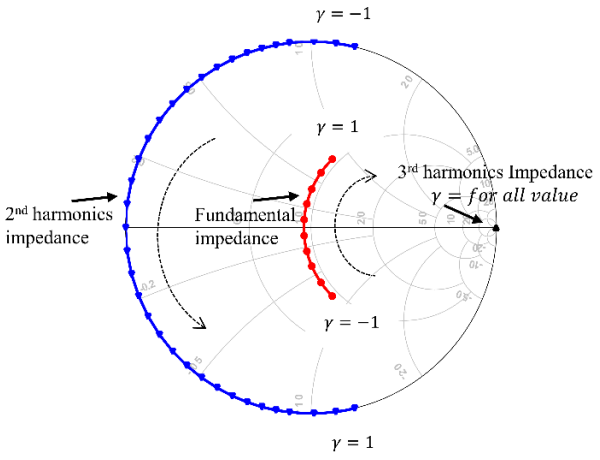

FIGURE 3. The theoretical impedance of fundamental, second, and third harmonic frequencies.

III. BROADBAND PA DESIGN METHODOLOGY

Based on the theoretical design space mentioned in Section II, the HTN and the fundamental frequency matching network are designed separately. In Figure 4, the schematic circuit of the proposed HTN is shown. The center frequency

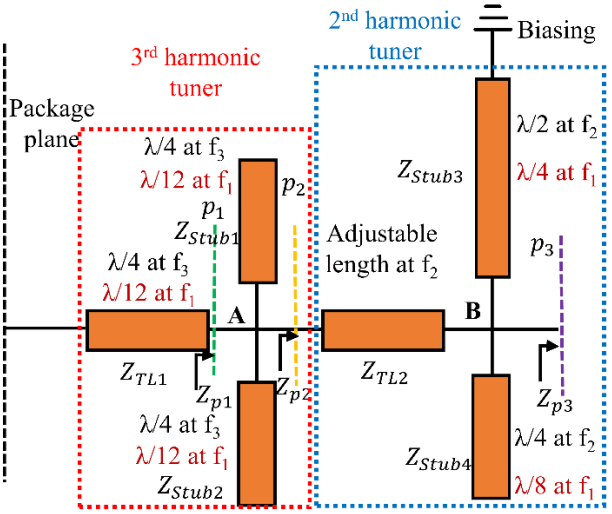

FIGURE 4. Proposed HTN up to third harmonics.

of the band is chosen in designing the HTN and the impedance buffer concept is also applied [23].

As shown in the dotted red box in Figure 4, shunt quarter-wave stubs (Stub1 and Stub2) are used to convert the impedance to the short circuit at point A. The electrical length of the shunt stub is calculated as:

$$\theta_{Stub1}^{@f_3} = \theta_{Stub2}^{@f_3} = 90^\circ \tag{5}$$

where the characteristic impedance of the shunt stub Z_{Stub1} and Z_{Stub2} is a free design parameter limited by achievable dimensions on the chosen substrate. The characteristic impedance is chosen to be the same for both stubs. In such a way, short-circuit impedance is achieved at point A. Then, the short circuit at point A is converted to an open circuit at the package plane using another transmission line, TL1. The length and the characteristic impedance of the transmission line are calculated by the following equation:

$$Z_{OMN}(f_3) = jZ_{TL1}\tan\theta_{TL1} \tag{6}$$

where $Z_{OMN}(f_3)$ is the optimum impedance at the third harmonics. For the ideal case, the optimum impedance at the package plane is infinite but practically, it is different. The characteristic impedance of the transmission line TL1 is also a free design parameter. Therefore, the transmission line's TL1 electrical length is calculated by the following equation:

$$\theta_{TL1} = \frac{\tan^{-1}(Z_{OMN}(f_3))}{jZ_{TL1}} \tag{7}$$

As shown in the blue dotted box in Figure 4, in order to achieve an optimum second-harmonic impedance termination, a quarter-wave open circuit stub (Stub 4) and a half-wave short circuit stub (Stub 3), together with an adjustable transmission line, TL2 is used to obtain optimum impedance at the package plane. The electrical lengths of the stubs are as follows:

$$\begin{aligned}\theta_{Stub3}^{@f_2} &= 180^\circ \\ \theta_{Stub4}^{@f_2} &= 90^\circ\end{aligned} \tag{8}$$

The characteristic impedance of the shunt stubs Z_{Stub3} and Z_{Stub4} are also free design parameters. The quarter-wave and half-wave stubs create the short circuit at point B at second harmonic frequency. Then, the transmission line's length TL2 is adjusted to convert the short circuit at the package plane from the point B together with the third HTN (shown as dotted red box). The half-wave stub at the second harmonics works as a quarter-wave stub at the fundamental frequency. It also converts the short circuit from the biasing point to open circuit at point B at the fundamental frequency. Therefore, the quarter-wave stub at fundamental frequency isolates the RF signal from the biasing.

The next step is to determine the dimensions of the adjustable transmission line, TL2. In order to find the length and impedance of the transmission line, TL2, the impedance at plane p_1 and the impedance at plane p_2 need to be derived first. The optimum impedance at the plane p_1 (shown as green dashed line in the red dotted box) is calculated as:

$$Z_{p1}(f_2) = Z_{TL1}\frac{Z_{OMN}(f_2) - jZ_{TL1}\tan\left(\theta_{TL1}^{@f_3}\cdot\frac{f_2}{f_3}\right)}{Z_{TL1} - jZ_{OMN}(f_2)\tan\left(\theta_{TL1}^{@f_3}\cdot\frac{f_2}{f_3}\right)} \tag{9}$$

The optimum impedance at the package plane p_2 (shown as orange dashed line in the in the red dotted box) is calculated as:

$$Z_{p2}(f_2) = \frac{Z_{p1}(f_2)Z_{Stub1}\cot\left(\theta_{Stub1}^{@f_3}\cdot\frac{f_2}{f_3}\right)}{2Z_{p1}(f_2) + Z_{Stub1}\cot\left(\theta_{Stub1}^{@f_3}\cdot\frac{f_2}{f_3}\right)} \tag{10}$$

Now, the TL2 transmission line electrical length is determined as follows:

$$\theta_{TL2} = \frac{\tan^{-1}(Z_{p2}(f_2))}{jZ_{TL2}} \tag{11}$$

where the characteristic impedance, Z_{TL2}, is also a free design parameter. Therefore, Equations 5 through 11 are used to determine all parameters of the HTN.

The next step is the design of the matching network for the fundamental frequency.

The optimum impedance at the fundamental frequency f_1 at the plane p_3(as shown as purple dashed line in the blue dotted box in Figure 4) is determined by applying the load-pull approach. The fundamental impedance matching network is then designed using the LPMT. The impedance-transforming structure of general form for the low pass matching is shown in Figure 5, where $g_0, g_1 \ldots\ldots g_n$ are the normalized component values. In designing the impedance transformer network, the most important parameters are the fractional bandwidth, w, the impedance transformation ratio, r, and the passband attenuation ripple, L_{Ar}. After determining these parameters, the next step is the determination of the number

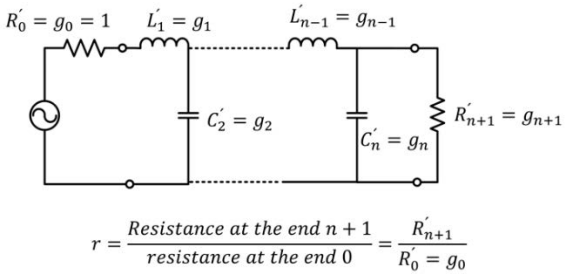

FIGURE 5. Low pass matching structure prototype.

of reactive elements needed for the matching network. Tables 1 to 5 in [24] can be used to find the needed value of n quickly. The normalized component value of the prototype is determined from the Chebyshev table (Table 6-10) in [24], then, at the desired system frequency, the prototype is scaled using the following equations:

$$\begin{aligned} R_K &= R'_K \left(\frac{R}{R'}\right) \\ C_K &= C'_K \left(\frac{\omega'_m}{\omega_m}\right)\left(\frac{R'}{R}\right) \\ L_K &= L'_K \left(\frac{\omega'_m}{\omega_m}\right)\left(\frac{R}{R'}\right) \end{aligned} \tag{12}$$

where R'_K, C'_K, and L'_K are the normalized design parameters and R_k, C_k, and L_k are the scaled design parameters. At high frequency, the lumped element is converted into transmission line using the Richards' transformation [25] given in equation (13):

$$\begin{aligned} Z_{in}^S &= jZ_o \tan \beta l \\ Z_{in}^o &= -jZ_o \cot \beta l \\ &= -jZ_o / \tan \beta l \end{aligned} \tag{13}$$

When the OMN, consisting of the HTN and fundamental impedance matching network, is obtained, then the IMN network is designed. At the time of designing the IMN, the optimum source impedance is determined using the source-pull technique. After that, the IMN is also designed using the LPMT.

IV. DESIGN IMPLEMENTATION

To validate the design methodology, the CCF RFPA is designed using the Cree CGH40010F device. The device is biased at 28 V, as suggested by the datasheet, and the biasing current is 60 mA as the class-F RFPA is operated at the class-B condition which normally operates at 10% to 15% of the maximum drain current. Before performing load-pull and source-pull, the stability and the biasing networks are designed. The parallel combination of the capacitor and resistor in the input matching network is used for low frequency stability. In addition to this, to improve stability, another resistor is added in series with the biasing line at the gate side. As for the biasing network, a quarter-wave transmission line

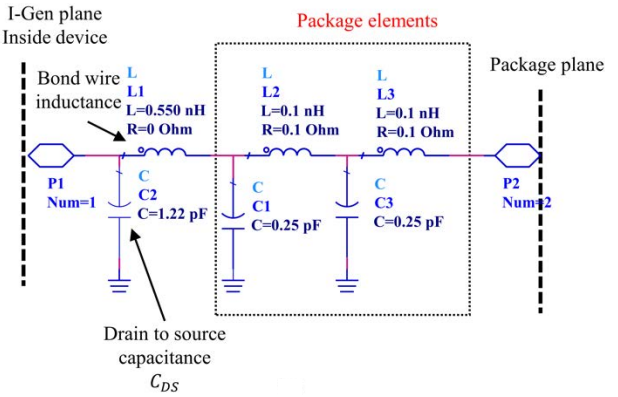

FIGURE 6. Output de-embedded network.

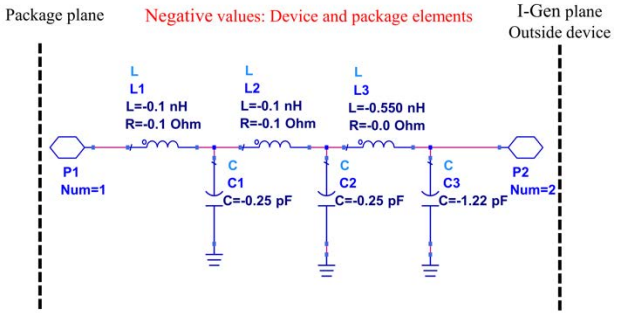

FIGURE 7. Mirror network of the de-embedded network.

and a radial stub are used. Then, load-pull and source-pull techniques are performed at the package plane of the Cree device to find out the optimal load and source impedances.

A. REALIZATION OF OMN

The OMN consists of the HTN and the fundamental matching network. Before designing the HTN, the optimum impedance at the I-Gen plane of the device is determined using the load pull approach in the Keysight Advanced Design Software (ADS) software. Then, HTN is designed using the methodology outlined in Section III. The free design parameters of the characteristic impedance of the transmission lines Z_{TL1}, Z_{TL2}, Z_{Stub1}, Z_{Stub2} and Z_{Stub4} are chosen to be 50 Ω. The characteristic impedance of Z_{Stub3} is chosen to be 90 Ω, which is higher than other stubs because this stub will be used for both as the matching element and as a quarter-wave biasing line at the same time. Therefore, a high impedance is better to be used in isolating the RF signal from the DC bias. The transmission line's electrical length at the package plane is calculated using Equations 5 to 11 and the center frequency of the band is chosen to be 3.8 GHz for calculating of the dimension of the transmission line. The lengths of the stubs are $\theta_{Stub1} = \theta_{Stub2} = 30^\circ$, $\theta_{Stub3} = 90^\circ$, $\theta_{Stub4} = 45^\circ$, $\theta_{TL1} = 45^\circ$, and $\theta_{TL2} = 9.55^\circ$.

The package and I-Gen planes are two different planes with an effect from the packaging parasitic capacitance and inductance between them. The output de-embedded network

is applied to CGH40100F [26], as shown in Figure 6, to obtain the optimum impedance at the I-Gen plane. When studying CCF modes, the correct waveforms at the I-Gen plane must be presented. Unfortunately, the waveform at the I-Gen plane is not accessible using the standard measurement system. In order to view the waveforms at the I-Gen plane, the de-embedding network and the mirror network with negative component values (as shown in Figure 7) are applied in the simulation. In this way, the I-Gen plane is translated to the package plane where the obtained impedances from the load pull simulation are applied. The HTN is designed carefully, considering the effect of parasitic elements after the I-Gen plane. A parasitic compensation network must be included in the HTN. As a result, the final HTN will be different from the theoretical one. The desired second and third harmonic impedances at the I-Gen plane are obtained by tuning the transmission length of TL1 and TL2. The final HTN together with the biasing network is shown in the dotted red and green box of Figure 9. With the HTN that have been designed, the optimum fundamental output impedance at the plane p_3 (as shown in Figure 4) is determined again using the load-pull technique. A center frequency of the band of 3.8 GHz is chosen for the designing of the OMN. The optimum output impedance of the device obtained at plane p_3 is 28.4 - j9.2 Ω at the center frequency of 3.8 GHz. The output matching of fundamental frequency has to be designed between 28.4 - j9.2 Ω and 50 Ω. The OMN for the fundamental frequency is implemented by applying the LPMT [24] using the optimum resistive impedance at the center frequency.

The remaining design steps of the fundamental frequency matching network are as follows:

First, the real-to-real impedance conversion at the fundamental frequency is applied. The real part of the fundamental load impedance is 28.4 Ω as obtained in the earlier step and the output terminating reference impedance used is 50 Ω. The impedance transformation ratio, r is obtained as follows:

$$r = \frac{terminating\ reference\ resistance\ at\ the\ output}{optimum\ resistance\ of\ the\ device}$$

The transformation ratio is 1.76. Therefore, the closest integer transformation ratio of $r = 2$ is chosen for prototype extraction. The calculated fractional bandwidth is 26.3%. A fractional bandwidth of 30% is chosen for the design of the matching network. The passband attenuation ripple, L_{Ar}, is selected to be less than 0.1 dB. The required order of the output matching is 4, determined from Tables 1 to 5 in [24].

Second step, the value of the normalized component of the matching network is calculated from Tables 6 to 10(e) in [24]. The normalized values of the components are shown in Figure 8.

Third step; this prototype is scaled at the center frequency chosen for this design that is 3.8 GHz and considering the 50 Ω system at the output of the RFPA (using Equation 12).

In the final step, the lump elements are converted into a transmission line using the Richards' transformation as described earlier. According to this theory, the capacitor

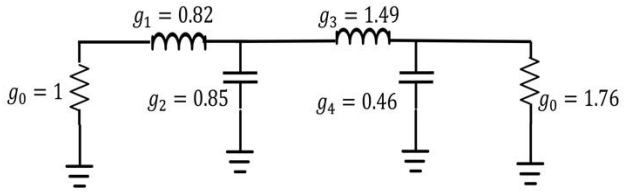

FIGURE 8. Normalized fundamental frequency matching network.

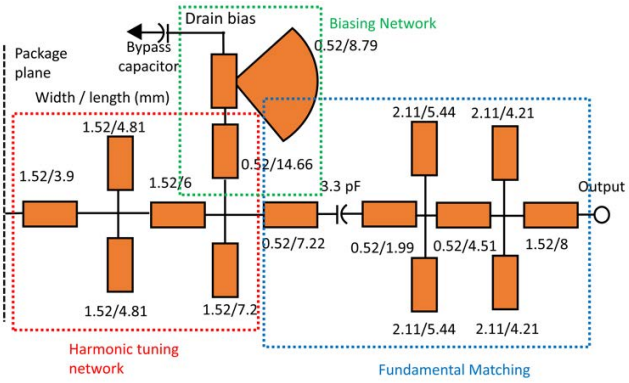

FIGURE 9. Output matching network.

is replaced by an open-circuited transmission line, and the inductor is replaced by the short-circuited transmission line. The length βl and characteristic impedance Z_0 of the transmission line is related by Equation 13. If the transmission line's length is short and has a high characteristic impedance, then its performance can be approximated to a series inductor. In contrast, when the transmission line's length is short and has a low characteristic impedance, then its performance can be approximated to a shunt capacitor [25]. This design is implemented on the Rogers 5880 substrate with a thickness of 0.51 mm and a dielectric constant of 2.2. The minimum width of the microstrip line corresponding to this substrate is 0.15 mm. Therefore, a characteristic impedance of 90 Ω corresponds to the line width of 0.52 mm is chosen for conversion of the inductor into the transmission line considering the minimum width and fabrication tolerance. The characteristic impedance of 40 Ω is chosen for the conversion of the capacitor to the microstrip line. The complete OMN is optimized together with the Cree transistor model to achieve optimum performances. The finalized dimension of the transmission line and stubs of the OMN are indicated in Figure 9.

The synthesized OMN load trajectories corresponding to the optimized OMN and the optimum load impedance of the Cree device for three frequencies (3.5 GHz, 3.8 GHz and 4.1 GHz) at the I-Gen plane are plotted on Smith chart, as shown in Figure 10. It is seen that the fundamental frequency is matched for a significantly wide bandwidth. The second harmonics and third harmonics impedances are located at the low impedance and the high impedance regions of the Smith chart, respectively. The result shows that the OMN performs well for a wide bandwidth on the proposed

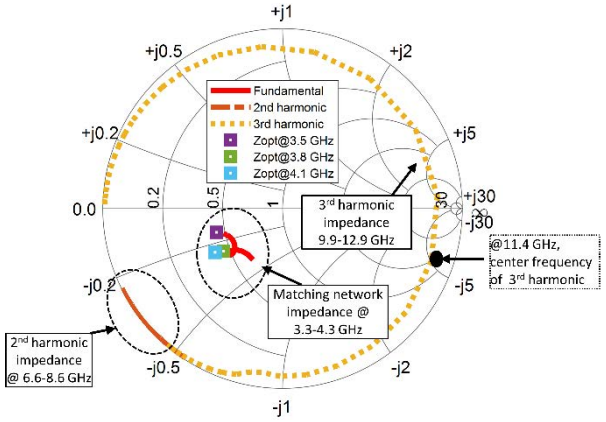

FIGURE 10. Impedance trajectories of the OMN at I-Gen plane.

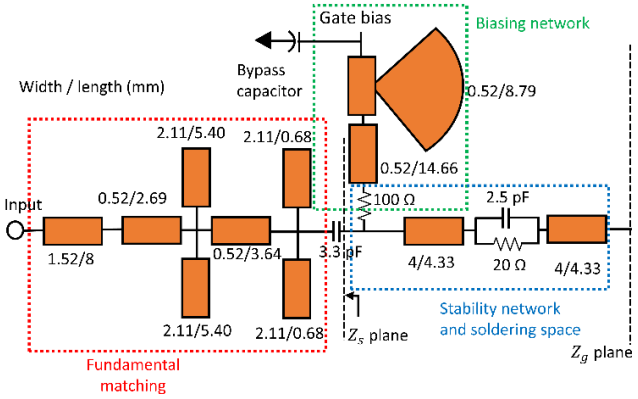

FIGURE 11. Input matching network.

design and this design maintains the desired impedance for the continuous class-F mode as described in Section II.

B. REALIZATION OF IMN

The IMN consists of a fundamental frequency matching network (red dotted box) and a stability network (blue dotted box) as shown in Figure 11. The stability network is designed using the parallel combination 20-Ω resistor and 2.5-pF capacitor (by-pass over the operating frequency band). Microstrip lines are added to provide soldering space for connecting the Cree device and the stability network which is also a part of the IMN.

The source impedance of the device at the Z_g plane (shown as purple dashed line) is different from the impedance at the Z_s plane (shown as orange dashed line) due the stability and biasing network of Figure 11. The source pull simulation is therefore performed at the Z_s plane. Since the input impedance matching at the harmonic's frequency plays a less critical role in enhancing the efficiency, therefore, only the fundamental frequency matching is considered and the higher harmonics are neglected. From the source pull simulation, the optimum source impedance obtained for the device at 3.8 GHz and at the Z_s plane is 106.1 + j 37.5 Ω. Using the same LPMT technique for the OMN, first, the real-to-real impedance transformation is performed. For the real impedance at center frequency of 106 Ω, the transformation ratio calculated is 2.12. Therefore, a transformation ratio of 2.2 is chosen for the design of the IMN. The required order is 4, calculated from the Tables 1 to 5 from [24]. The normalized component of the prototype matching network is obtained from [24]. Then, the scaling and the lump element conversion need to be performed. The final optimized parameter of the IMN is shown in Figure 11.

V. SIMULATION AND EXPERIMENTAL RESULT

A. SIMULATED VOLTAGE AND CURRENT WAVEFORM

To validate the designed RFPA's CCF operating mode, the voltage and current wave at the I-Gen plane are investigated using the Keysight ADS. The de-embedded voltage and current waveform at the lower edge of the band, 3.5 GHz, at the center of the band, 3.8 GHz, and at the upper edge of the band, 4.1 GHz at the I-Gen plane are shown in Figure 12. It is observed that the waveform confirms the CCF mode of RFPA as the current waveform is approximately half rectified sine wave and voltage waveforms are close to the theoretical continuous class-F voltage waveform, as shown in Figure 2. To further validate the RFPA is operating in the CCF mode, the RFPA is also simulated below 3.3 GHz.

B. S-PARAMETER MEASUREMENT RESULT

Figure 13 shows the small-signal S-parameters of the simulated circuit and the measured S-parameters of the fabricated RFPA. The S-parameters were measured using the Agilent PNA N5227A microwave network analyzer. The instrument was calibrated using the Agilent N4694-60001, an electronic calibration module and the experiment is set up for a broadband frequency sweep from 10 MHz to 6 GHz. The simulated and measured results line up reasonably well. The measured gain is between 10 dB and 10.9 dB for the band of frequency of 3.3 to 4.3 GHz.

C. CONTINUOUS WAVE (CW) MEASUREMENT

The performance of the fabricated RFPA is also measured with a CW signal over the band starting from 3.3 GHz to 4.3 GHz with a step of 0.1 GHz. AnaPico APSIN12G signal generator is used as an input source for the RFPA and boosted by a commercially available driver power amplifier (Mini-Circuit ZVE-8G+) to provide sufficient input power. The output power of RFPA is measured using an Agilent U2044XA power sensor. The fabricated broadband RFPA is shown in Figure 14.

The CW measurement setup of the designed RFPA is shown in Figure 15. Two power supplies are used for the driver RFPA and the designed RFPA. The positive and negative voltage is applied to the drain and the gate of the device, respectively. The RF input power of different frequencies from 3.3 GHz to 4.3 GHz with a step size of 0.1 GHz

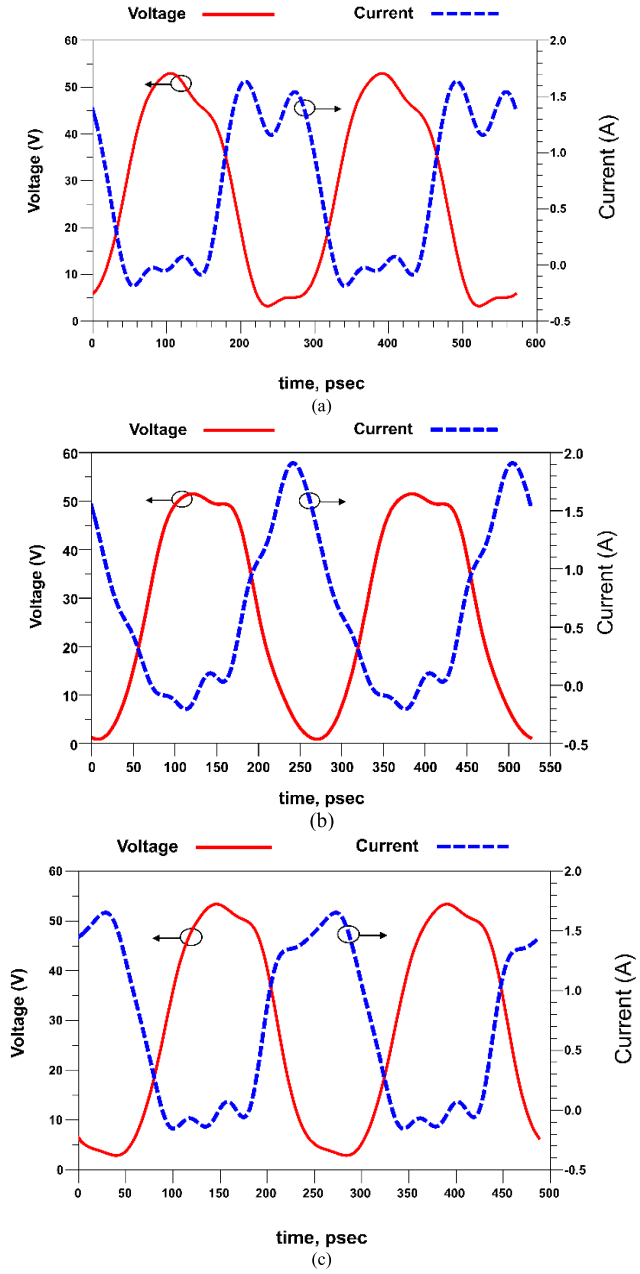

FIGURE 12. At the I-Gen plane, the Voltage and current waveform at (a) 3.5 GHz (b) 3.8 GHz and (c) 4.1 GHz.

is applied to the designed RFPA and the measurement is recorded at the output.

Figure 16 depicts drain efficiency (DE), power added efficiency (PAE), and gain over the frequency band. All the data is plotted at 40 dBm (±0.3 dBm) output power. The measured DE is found to be greater than 55.9% in the whole operating range with a maximum of 65.3%. The PAE varies in a pattern similar to that of the DE, but the PAE has a lower value than DE as at the time of calculating the PAE, the DC input power is not included., In the whole frequency band, the gain was greater than 7.8 dB at 4.3 GHz with a maximum of 11.1 dB at 3.8 GHz It is noted that the measured DE and PAE are

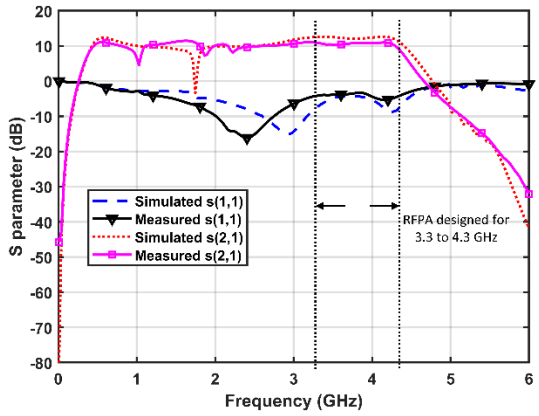

FIGURE 13. Simulated and measured S-parameter comparison.

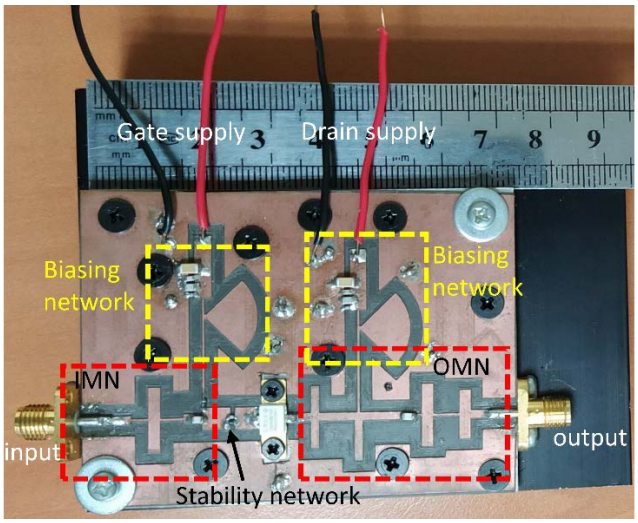

FIGURE 14. Photo of the realized CCF 10 W power amplifier (73 × 55 mm^2).

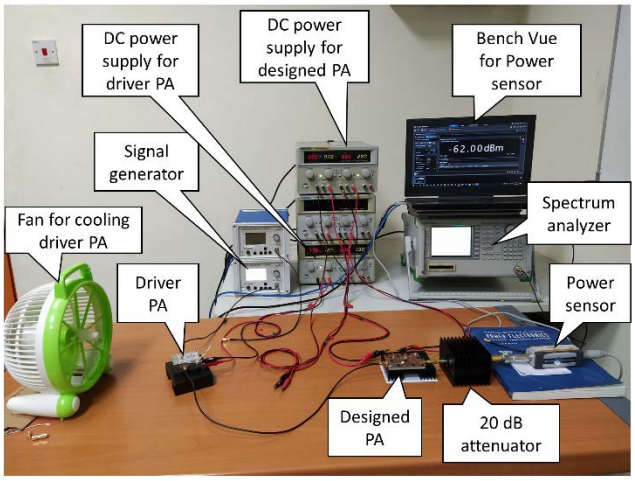

FIGURE 15. Measurement setup for CW signal.

better than the simulated results at most frequency points and the differences are between 0% to 12% which is within the expected error of a reasonably good non-linear model.

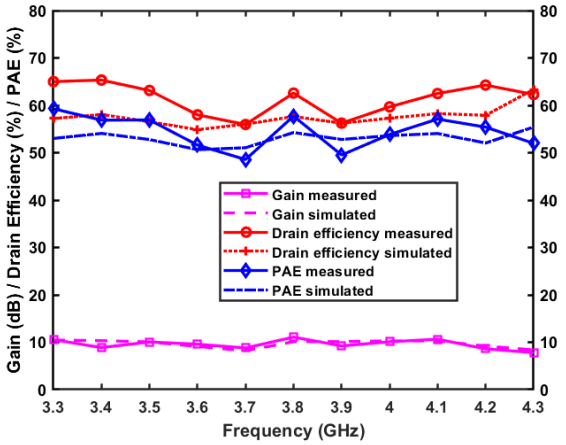

FIGURE 16. Gain, Drain Efficiency and PAE at 40 dBm (±0.3 dBm) output power for whole bandwidth.

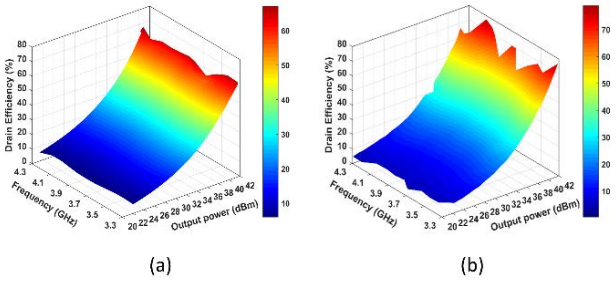

FIGURE 17. Drain efficiency at different output power and frequency (a) simulation result and (b measured result).

The simulated and measured drain efficiency at different output power and frequency is shown in Figure 17 (a) and (b). From the measurement data of Figure 17(b), it is seen that the output power decreases rapidly as the power is backed-off from the *Psat* value. This is an expected behavior for the Continuous Class-F RFPAs, as confirmed in literature [14], [27], [28]. The maximum measured efficiency reaches at a peak of 78% at 4.1 GHz with 41.9 dBm output power. The efficiency is higher than 55.9% at 40 dBm (± 0.3 dBm) over the whole bandwidth of 3.3 GHz to 4.3 GHz.

Figure 18(a) shows the measured gain versus output power at three frequencies: 3.5 GHz, 3.8 GHz and 4.1 GHz to characterize the performance over the bandwidth. From the plot, the RFPA is observed to be linear up to the 40 dBm output power and compressed by 1dB at 41.7 dBm, 42.5 dBm and 42.3 dBm output power at 3.5 GHz, 4.1 GHz and 4.3 GHz, respectively. It is observed that the measured gain fluctuates, at some frequencies, the gain is higher and at some frequencies, the gain is slightly lower. In Figure 18(b), the output power versus input power is shown for all frequencies in the interested band. These two figures confirmed that the RFPA behaves linearly up to the nominal 40 dBm (10W) output power. The gain starts to compress above the 40 dBm output power.

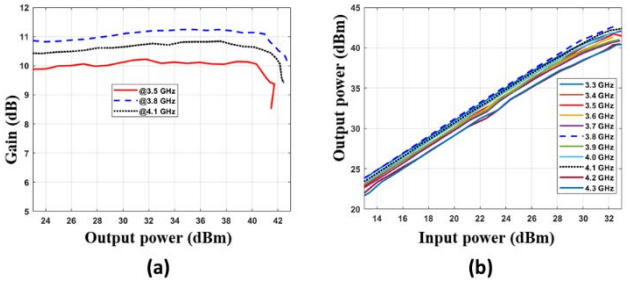

FIGURE 18. (a) Gain versus output power at 3.5 GHz, 3.8 GHz and 4.3 GHz frequencies (b) Output power versus input power.

Table 1 compares the designed RFPA with a state-of-the-art broadband RFPAs with Cree CGH40010F device and shows the proposed RFPA operates at the highest operating frequency with 1 GHz bandwidth compared to other RFPAs with comparable performances. The output power variation is small compared to the published literatures in [7], [10], [12], and [29]. The DE is very good at this frequency band that varies from 55.9% to 65.3%, as normally the efficiency decreases with the rise of operating frequency for the Cree device.

TABLE 1. Comparison with state-of-the-art broadband RFPAs.

Ref.	Year	Class	Bandwidth (GHz)	P_{out} dBm	DE (%)
[7]	2017	CCF	0.4–2.3	39–42	62.3–80.5
[8]	2017	CCF	1.4–2.4	>40	60–73
[12]	2018	CCF	1.2–3.6	40–42.2	60–72
[10]	2019	CCF	1.7–3.0	39.7–41.1	54.7–74.8
[29]	2021	CCF^{-1}	0.5-2.5	38.8-41.9	60.7-71.5
This work	2022	CCF	3.3–4.3	39.9–40.3	55.9–65.3

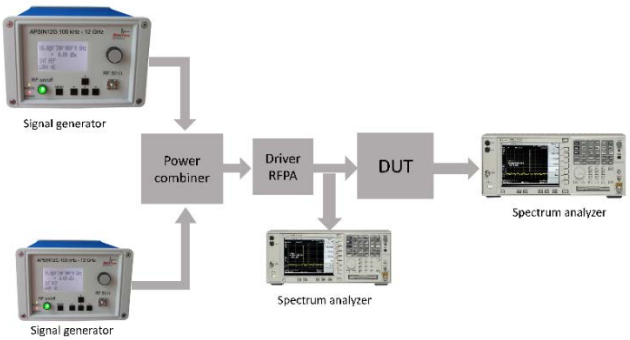

FIGURE 19. Measurement setup for the two-tone test.

D. LINEARITY CHARACTERISTIC WITH A TWO-TONE SIGNAL

To assess the linearity of the fabricated RFPA, the input is fed with two-tone signals with a frequency of 10 MHz

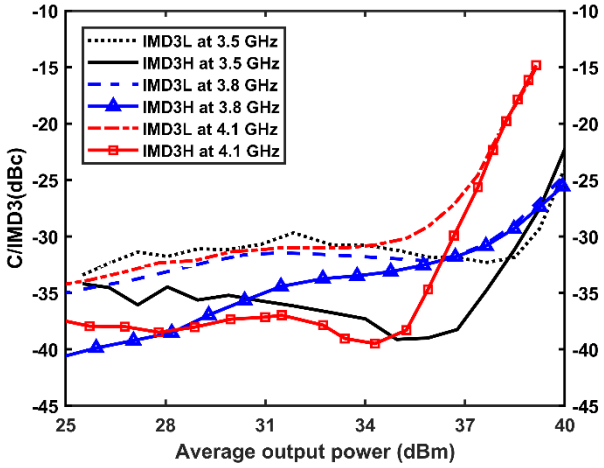

FIGURE 20. Measured C/IMD3 at 3.5 GHz, 3.8 GHz, and 4.1 GHz.

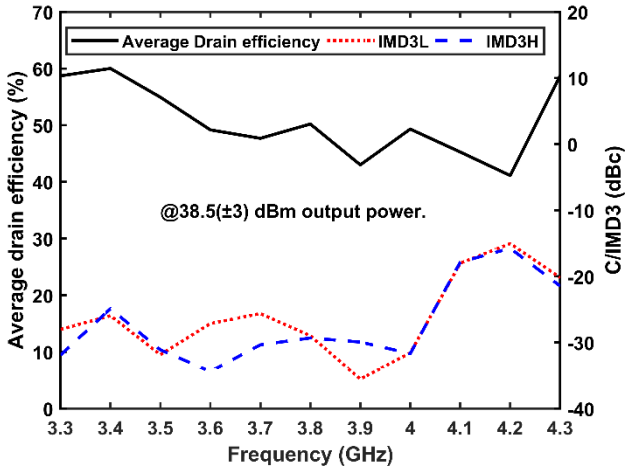

FIGURE 21. Drain efficiency and C/IMD3 vs frequency.

spacing. The measurement setup for a two-tone signal test is shown in Figure 19. When a two-tone signal is applied then the RFPA will generate a mixing product of two signals which are called the intermodulation distortion (IMD) products. The common way of removing IMD is filtering. As third-order intermodulation distortion (IMD3) products ($2f_1 - f_2$ and $2f_2 - f_1$) are very near to the fundamental tone, it cannot be filtered out easily. Therefore, the main contributor to the signal distortion is IMD3. Therefore, linearity is measured in terms of the difference of power level between the fundamental tone and the third harmonics tone. The carrier to third-order intermodulation suppression ratio (C/IMD3) is plotted against average output power for three frequencies: at the middle of the lower band (3.5 GHz); at the center of the band (3.8 GHz); and at the middle of the upper band (4.1 GHz), as shown in Figure 20. The RFPA performs better at the lower frequency compared to the higher frequency within the band. The C/IMD3 for both middle of the lower side of the band and center frequency of the bands are less than −23 dBc up to average output power of 40 dBm, and it is less than −15 dBc for the center frequency of the upper bands until 39 dBm average output power, as shown in Figure 20.

Next, to characterize the linearity performance of the designed RFPA over the whole frequency band, a two-tone signal with 10 MHz spacing is applied from 3.3 GHz to 4.1 GHz frequency at 38.5(±0.3) dBm average output power and the linearity performance of the RFPA is plotted in Figure 21. At the lower frequency of the band, the linearity is somewhat better compared to the higher frequency. Across the entire band, the C/IMD3 is less than -15 dBc, with a minimum of -35 dBc at 3.9 GHz frequency. The average drain efficiency is between 42% and 60% (as shown in Figure 21), which is good at 38.5 dBm average output power, as it is a 40 dBm device. From these two figures (Figure 20 and Figure 21), it is noted that the C/IMD3 versus output power shows that the performance is not good as the output power increases, especially for the C/IMD3 at 4.1 GHz and higher. The asymmetry of the lower IMD3 sideband (IMD3L) and the higher IMD3 sideband (IMD3H) is also not desirable. This linearity performance will be investigated in a separate work.

VI. CONCLUSION

The wideband CCF RFPA is presented here using a GaN HEMT 10W device for the frequency band 3.3 GHz to 4.3 GHz. To maintain the high efficiency of the designed RFPA, a HTN and a wideband matching network using LPMT for the fundamental frequency are applied in sequence within the OMN. The drain efficiency achieved is quite significantly good between 55.9% and 65.3% considering the 1 GHz bandwidth, while the output power variation is between 39.9 to 40.3 dBm. The C/IMD3 is less than -15 dBc for the whole frequency band at 38.5 dBm output power. In terms of linearity, the performance of the RFPA is not very good and more investigations will be done in a separate work. Some techniques such as the digital predistortion can be applied to get better linearity performances. The overall performances and specifically the broadband characteristics of the proposed RFPA confirm that it can be used in the transmitter of a 5G wireless communication system especially for the 3.3 to 4.3 GHz band.

REFERENCES

[1] Y. Dong, L. Mao, and S. Xie, "Extended continuous inverse class-F power amplifiers with class-AB bias conditions," *IEEE Microw. Wireless Compon. Lett.*, vol. 27, no. 4, pp. 368–370, Apr. 2017.

[2] G. Ancans, V. Bobrovs, A. Ancans, and D. Kalibatiene, "Spectrum considerations for 5G mobile communication systems," *Proc. Comput. Sci.*, vol. 104, pp. 509–516, Jan. 2017.

[3] M. G. Sadeque, Z. Yusoff, and M. Roslee, "A high-efficiency continuous class-F power amplifier design using simplified real frequency technique," *Bull. Electr. Eng. Informat.*, vol. 9, no. 5, pp. 1924–1932, Oct. 2020.

[4] K. K. Sessou. (2014). *Design of a Class-F Power Amplifier With Reconfigurable Output Harmonic Termination in 0.13 µm CMOS*. Iowa State University. [Online]. Available: http://lib.dr.iastate.edu/cgi/viewcontent.cgi?article=4670&context=etd

[5] V. Carrubba, M. Akmal, R. Quay, J. Lees, J. Benedikt, S. C. Cripps, and P. J. Tasker, "The continuous inverse class-F mode with resistive second-harmonic impedance," *IEEE Trans. Microw. Theory Techn.*, vol. 60, no. 6, pp. 1928–1936, Jun. 2012.

[6] H. Huang, B. Zhang, C. Yu, J. Gao, Y. Wu, and Y. Liu, "Design of multioctave bandwidth power amplifier based on resistive second-harmonic impedance continuous class-F," *IEEE Microw. Wireless Compon. Lett.*, vol. 27, no. 9, pp. 830–832, Sep. 2017.

[7] Q.-H. Tang, Y.-H. Li, and W.-G. Li, "Over second octave power amplifier design based on resistive–resistive series of continuous class-F/F^{-1} modes," *IEEE Microw. Wireless Compon. Lett.*, vol. 27, no. 5, pp. 494–496, May 2017.

[8] E. Aggrawal, K. Rawat, and P. Roblin, "Investigating continuous class-F power amplifier using nonlinear embedding model," *IEEE Microw. Wireless Compon. Lett.*, vol. 27, no. 6, pp. 593–595, Jun. 2017.

[9] T. Wang, Z. Cheng, G. Liu, S. Li, and Z. Zhang, "Highly efficient broadband continuous inverse class-F power amplifier using multistage second harmonic control output matching network," *Int. J. RF Microw. Comput.-Aided Eng.*, vol. 30, no. 5, pp. 1–8, May 2020.

[10] G. Liu, F. Mu, X. Qiu, Y. Leng, and X. Peng, "Design of broadband power amplifier based on continuous class-F mode with frequency parameterization," *IEICE Electron. Exp.*, vol. 16, no. 6, pp. 1–4, Mar. 2019.

[11] Z. Yang, Y. Yao, Z. Liu, M. Li, T. Li, and Z. Dai, "Design of high efficiency broadband continuous class-F power amplifier using real frequency technique with finite transmission zero," *IEEE Access*, vol. 6, pp. 61983–61993, 2018.

[12] C. Huang, S. He, W. Shi, and B. Song, "Design of broadband high-efficiency power amplifiers based on the hybrid continuous modes with phase shift parameter," *IEEE Microw. Wireless Compon. Lett.*, vol. 28, no. 2, pp. 159–161, Feb. 2018.

[13] E. Aggrawal, S. Saxena, and K. Rawat, "Broadband power amplifier design by exploring design space of continuous class-F mode," in *Proc. Asia–Pacific Microw. Conf. (APMC)*, Dec. 2016, pp. 4–7.

[14] N. Tuffy, L. Guan, A. Zhu, and T. J. Brazil, "A simplified broadband design methodology for linearized high-efficiency continuous class-F power amplifiers," *IEEE Trans. Microw. Theory Techn.*, vol. 60, no. 6, pp. 1952–1963, Jun. 2012.

[15] M. Alizadeh and D. Rönnow, "A two-tone test for characterizing nonlinear dynamic effects of radio frequency amplifiers in different amplitude regions," *Measurement*, vol. 89, pp. 273–279, Jul. 2016.

[16] M. G. Sadeque, Z. Yusoff, M. Roslee, and N. S. R. Hadi, "Design of a broadband continuous class-F RF power amplifier for 5G communication system," in *Proc. IEEE Regional Symp. Micro Nanoelectron. (RSM)*, Aug. 2019, pp. 145–148.

[17] K. Chen and D. Peroulis, "Design of broadband highly efficient harmonic-tuned power amplifier using in-band continuous class-F^{-1}/F mode transferring," *IEEE Trans. Microw. Theory Techn.*, vol. 60, no. 12, pp. 4107–4116, Dec. 2012.

[18] O. Ceylan, H. B. Yağci, and S. Paker, "Tunable class-F high power amplifier at X-band using GaN HEMT," *Turkish J. Electr. Eng. Comput. Sci.*, vol. 26, no. 5, pp. 2327–2334, Sep. 2018.

[19] F. H. Raab, "Class-F power amplifiers with maximally flat waveforms," *IEEE Trans. Microw. Theory Techn.*, vol. 45, no. 11, pp. 2007–2012, Nov. 1997.

[20] F. H. Raab, "Maximum efficiency and output of class-F power amplifiers," *IEEE Trans. Microw. Theory Techn.*, vol. 49, no. 6, pp. 1162–1166, Jun. 2001.

[21] V. Carrubba, A. L. Clarke, M. Akmal, J. Lees, J. Benedikt, P. J. Tasker, and S. C. Cripps, "The continuous class-F mode power amplifier," in *Proc. 5th Eur. Microw. Integr. Circuits Conf.*, Paris, France, Sep. 2010, pp. 432–435.

[22] S. C. Cripps, P. J. Tasker, A. L. Clarke, J. Lees, and J. Benedikt, "On the continuity of high efficiency modes in linear RF power amplifiers," *IEEE Microw. Wireless Compon. Lett.*, vol. 19, no. 10, pp. 665–667, Oct. 2009.

[23] S. Zheng, Z. Liu, X. Zhang, X. Zhou, and W. Chan, "Design of ultrawideband high-efficiency extended continuous class-F power amplifier," *IEEE Trans. Ind. Electron.*, vol. 65, no. 6, pp. 4661–4669, Jun. 2018.

[24] G. L. Matthaei, "Tables of Chebyshev impedance–transforming networks of low-pass filter form," *Proc. IEEE*, vol. 52, no. 8, pp. 939–963, Aug. 1964.

[25] D. M. Pozar, *Microwave Engineering*, 4th ed. Hoboken, NJ, USA: Wiley, 2012.

[26] P. Wright, "Development of novel design methodologies for the efficiency enhancement of RF power amplifiers in wireless communications," Ph.D. Thesis, School Eng., Cardiff Univ., Cardiff, U.K., 2010.

[27] Z. Yang, Y. Yao, M. Li, Y. Jin, T. Li, Z. Geng, and Z. Yu, "A precise harmonic control technique for high efficiency concurrent dual-band continuous class-F power amplifier," *IEEE Access*, vol. 6, pp. 51864–51874, 2018.

[28] M. Shariatifar, M. Jalali, and A. Abdipour, "A concurrent dual-band continuous class-F power amplifier with intermodulation impedance tuning: Analysis and design technique," *AEU-Int. J. Electron. Commun.*, vol. 111, Nov. 2019, Art. no. 152899.

[29] C. Ni, H. Wang, J. Liu, M. Chen, Z. Zhang, L. Zhang, J. Zhu, and X. Wu, "A broadband high-efficiency hybrid continuous inverse power amplifier based on extended admittance space," *Frontiers Phys.*, vol. 9, pp. 1–7, Jul. 2021.

MD. GOLAM SADEQUE (Member, IEEE) received the B.Sc. (Eng.) degree in electrical and electronics engineering (EEE) from the Rajshahi University of Engineering and Technology (RUET), in 2011, and the Master of Engineering Science (M.Eng.Sc.) degree from the Faculty of Engineering, Multimedia University (MMU), Malaysia, in 2022. He is currently working as an Assistant Professor with the Department of EEE, Pabna University of Science and Technology (PUST), Pabna, Bangladesh. His research interests include the design of radio frequency power amplifier (RFPA) and biomedical engineering.

ZUBAIDA YUSOFF (Senior Member, IEEE) received the B.Sc. degree *(cum laude)* in electrical and computer engineering and the M.Sc. degree in electrical engineering from The Ohio State University, USA, in 2000 and 2002, respectively, and the Ph.D. degree, in 2012. She holds the position of a Senior Lecturer at the Faculty of Engineering, Multimedia University. She worked with Telekom Malaysia International Network Operation, in 2002, before she joined Multimedia University, in 2004. She continued her studies at Cardiff University, Wales, U.K., in 2008. She has presented technical papers at conference nationally and internationally. One of her conference papers has received "Honorable Mention" for the Student Paper Competition at the International Microwave Symposium, USA, in 2011. She has authored/coauthored more than 25 journals and conference papers. Her research interests include the area of microelectronics, analog/mixed signal, RF circuit design, and microwave/mm-wave power amplifier systems.

SHAIFUL JAHARI HASHIM received the B.Eng. degree in electrical and electronics engineering from the University of Birmingham, U.K., in 1998, the M.Sc. degree from the National University of Malaysia, in 2003, and the Ph.D. degree from Cardiff University, U.K., in 2011. He is currently an Associate Professor with the Department of Computer and Communication Systems Engineering, Faculty of Engineering, Universiti Putra Malaysia (UPM). His research interests include cloud computing, the Internet of Things (IoT), network security, and nonlinear wireless measurement systems.

AZAH SYAFIAH MOHD MARZUKI (Senior Member, IEEE) received the B.Eng. degree (Hons.) in electronics from Multimedia University, Cyberjaya, in 2002, and the M.Sc. degree in communications engineering from Durham University, U.K., in 2008. She has been a Professional Engineer (P.Eng.) and a Researcher at TM R&D Sdn Bhd, since 2002. She has 18 years of experience in wireless technology research mainly in RF, microwave and mm-wave module and transceiver design, testing, and development. Her research interest includes connectivity solutions for high-speed internet. She served as an Executive Committee for IEEE Malaysia Section, in 2019, and IEEE Malaysia Joint Chapter AP/MTT/EMC.

JONATHAN LEES (Senior Member, IEEE) received the M.Sc. and Ph.D. degrees in electronic and microwave engineering from Cardiff University, U.K., in 2002 and 2006, respectively.

He is currently the Head of the Department for Electrical and Electronic Engineering, Cardiff School of Engineering, Cardiff University, and a Reader of the Centre for High Frequency Engineering (CHFE). His key research interests include linear-efficient PA design and characterization with a specific interest in the design and optimization of high-efficiency power amplifiers. His work in this area culminated in the first published GaN Doherty amplifier. His research interests include the development of novel high-power, broadband time-domain measurement and load-pull techniques, compound semiconductor electronics and investigation into RF properties of materials, microwave heating, and novel applications of microwave engineering.

DOMINIC FITZPATRICK (Senior Member, IEEE) received the B.Sc. and M.Sc. degrees in solid state microwave physics from the University of Portsmouth, U.K., and the Ph.D. degree from Cardiff University, Wales. He has been involved with the design of solid-state RF & microwave amplifiers for over 35 years. He has been the Technical Director of two U.K. companies designing and manufacturing SSPAs. In 2010, he founded Powerful Microwave, a consultancy specializing in the design and manufacture of solid-state microwave amplifiers. Since 2019, he has been the Head of Amplifier Development at Ametek-CTS, responsible for the design and development activities of their power amplifiers ranging from 4 kHz to over 40 GHz.